

Global Biogeochemical Cycles®

RESEARCH ARTICLE

10.1029/2025GB008532

Key Points:

- The concentration of dissolved black carbon (DBC) was mainly controlled by mixing processes in three Chinese estuaries
- Input and removal of DBC were observed during flood and ebb tides, respectively
- Submarine groundwater discharge accounts for ~16–23% of riverine DBC flux to the ocean

Supporting Information:

Supporting Information may be found in the online version of this article.

Correspondence to:

H. Bao,
baohy@xmu.edu.cn

Citation:

Zhao, W., Bao, H., Peng, L., Du, M., Li, K., Zhan, X., et al. (2025). Transport of dissolved black carbon in three estuaries in China: Roles of flood-ebb tides and Submarine groundwater discharge. *Global Biogeochemical Cycles*, 39, e2025GB008532. <https://doi.org/10.1029/2025GB008532>

Received 5 FEB 2025
Accepted 23 MAY 2025

Author Contributions:

Data curation: Lejin Peng, Keyuan Li
Formal analysis: Moge Du, Jin-Yu Terence Yang
Funding acquisition: Hongyan Bao, Shuh-Ji Kao
Investigation: Keyuan Li, Xiaoqian Zhan, Dekun Huang, Wenbin Zou
Methodology: Moge Du, Li Tian
Resources: Dekun Huang
Supervision: Hongyan Bao
Writing – review & editing: Hongyan Bao, Lejin Peng, Keyuan Li, Xiaoqian Zhan, Shuwen Li

Transport of Dissolved Black Carbon in Three Estuaries in China: Roles of Flood-Ebb Tides and Submarine Groundwater Discharge

Weiqliang Zhao^{1,2}, Hongyan Bao^{1,3} , Lejin Peng¹, Moge Du⁴, Keyuan Li¹, Xiaoqian Zhan¹, Shuwen Li¹, Li Tian¹, Dekun Huang^{5,6} , Wenbin Zou¹, Jin-Yu Terence Yang¹ , and Shuh-Ji Kao⁷

¹State Key Laboratory of Marine Environmental Science, College of Ocean and Earth Sciences, Xiamen University, Xiamen, China, ²Fourth Institute of Oceanography, Ministry of Natural Resources, Beihai, China, ³Fujian Provincial Key Laboratory for Coastal Ecology and Environmental Studies, Xiamen University, Xiamen, China, ⁴Graduate School of Oceanography, University of Rhode Island, Narragansett, RI, USA, ⁵Third Institute of Oceanography, Ministry of Natural Resources, Xiamen, China, ⁶Observation and Research Station of Island and Coastal Ecosystems in the Western Taiwan Strait, Ministry of Natural Resources, Xiamen, China, ⁷State Key Laboratory of Marine Resource Utilization in South China Sea, Hainan University, Haikou, China

Abstract Estuaries are essential for the ocean's mass balance of terrestrial dissolved organic matter (DOM). Dissolved black carbon (DBC) constitutes the largest known persistent fraction of DOM in marine environments. However, the alterations of DBC during its transport through estuaries remain largely unknown. In this study, we conducted six sampling cruises across three estuaries in China, which varied in size, tidal patterns, and hydrological conditions. We measured DBC concentrations in both the overlying water and sediment porewater. Our results indicated that DBC input occurred during flood tides, whereas DBC removal was observed during ebb tides. Modeling results and laboratory experiments suggest that photodegradation and photo-dissolution were not the primary mechanisms influencing these patterns; instead, variations in submarine groundwater discharge (SGD) of DBC may account for the observed flood-ebb-related fluctuations. Additionally, we found a higher internal accumulation of DBC during the lower runoff period in the three estuaries, which could be related to the longer flushing time. We estimated that SGD-derived DBC flux accounted for ~12% of DBC discharged from the Jiulong River to the estuary, and represented ~16–23% of riverine DBC discharge on a global scale. Our study provides new insights into the flood-ebb-tides-related DBC transport in estuaries, which should be considered in future studies of other DOM components in the estuarine region. Furthermore, our study underscores the significance of SGD flux in the transport of terrestrial DOM to the ocean, highlighting the need for its incorporation into the global budget of terrestrial organic matter.

Plain Language Summary Estuaries play an important role in transferring terrestrial organic matter from land to the ocean. One key component, dissolved black carbon (DBC), is a long-lasting organic matter component in seawater. However, how DBC changes while moving through estuaries is not well understood. In this study, we collected samples from three different estuaries in China, which varied in size, tides, and river discharge level. We measured DBC in both the water column and sediment porewater. Our results showed that DBC concentrations showed an input trend during flood tides (when water flows into the estuary) and a removal trend during ebb tides (when water flows out). We think this is because the flood tide promotes DBC release from the submarine groundwater into the water column, while the ebb tide may limit this process. Overall, our study shows that estuaries are an important source of DBC, contributing ~20% of the riverine DBC that enters the ocean each year. This highlights the need to consider estuarine sources when calculating the global dissolved black carbon balance.

1. Introduction

Incomplete combustion of biomass and fossil fuels generates significant amounts of CO₂, meantime, it leads to the formation of a continuum of thermally altered organic matter. Among these, the condensed aromatics exhibit a higher resistance to biodegradation (Bostick et al., 2021; Kuzyakov et al., 2014) and persist much longer than other thermally altered components, such as levoglucosan (Coppola et al., 2019, 2024; Ziolkowski & Druffel, 2010). A portion of condensed aromatics can then dissolve in the water after the modifications by biotic and abiotic processes, referred to as dissolved black carbon (DBC) (Hockaday et al., 2007; Roebuck et al., 2017).

DBC represents the largest known stable dissolved organic carbon (DOC) pool in the ocean (Dittmar & Paeng, 2009) and plays a critical role in the global carbon cycle, being sensitive to both anthropogenic disturbances (such as land-use change and deforestation) and climate change (e.g., increased wildfires) (Coppola et al., 2022). Understanding the cycling and regulatory factors of DBC within the Earth system is essential for predicting its future changes in the context of global climate change.

Current estimates suggest that riverine discharge is the primary source of DBC to the ocean (Coppola et al., 2022; Jones et al., 2020). However, a notable 6‰ discrepancy in the stable carbon isotopes of DBC between river and sea waters indicates that other unidentified sources and/or extensive processing during transport to the ocean may be significant (Wagner et al., 2019). Estuaries are the only way for riverine organic matter to the sea, where complex biogeochemical processing of terrestrial organic matter occurs (Canuel & Hardison, 2016). Under controlled conditions, ultraviolet (UV) light has been shown to efficiently remove DBC (Stubbins et al., 2012); however, in natural environments, the presence of particles can scatter a substantial portion of UV light (Cao et al., 2018), thereby limiting the impact of photodegradation on DBC. Conversely, photodissolution from particles may increase DBC in the water column (Roebuck et al., 2017). In addition, other sources such as submarine groundwater discharge (SGD) and porewater exchange are non-negligible for providing water and DOC to the ocean (Du et al., 2024; Hong et al., 2017; Reithmaier et al., 2023). The global SGD flux of DOC from coastal salt marsh and mangroves was estimated to be $\sim 27 \text{ Tg yr}^{-1}$, which is more than 10% of global riverine discharge (Hedges et al., 1997; Reithmaier et al., 2023). Dittmar et al. (2012) also observed the export of DBC from a fire-impacted wetland. The net seaward flux of DBC is thus the result of these various processes and sources.

Given the significance of estuaries, several studies have been conducted to elucidate the distribution and influencing factors of DBC within these ecosystems (Mannino & Harvey, 2004; Marques et al., 2017; Q. Zhang, Zhou, et al., 2023; Zhao et al., 2023). A recent study indicated that approximately 20% of DBC was removed in a small subtropical estuary (Zhao et al., 2023). Similarly, it was suggested that over 50% of DBC was removed in Arctic river estuaries and coastal regions (Z. Fang, Huang, et al., 2021). In contrast, apparent input of DBC was observed in the Delaware and Pearl River estuaries (Mannino & Harvey, 2004; Q. Zhang, Zhou, et al., 2023), suggesting contributions from internal sources. Furthermore, unidentified sources of DBC, beyond riverine input and atmospheric deposition, have been observed in coastal seas (Bao et al., 2023). Globally, the input rate of DBC is significantly lower than its removal rate (Yamashita et al., 2022). Even considering hydrothermal-derived DBC (Yamashita et al., 2023), an imbalance persists, indicating the existence of “missing sources” of DBC that have yet to be accurately quantified in coastal seas and the open ocean.

The observed differences in input/removal patterns and the lack of understanding regarding the influencing factors necessitate more comprehensive studies. However, most research has been conducted within individual estuaries and often lacks sufficient temporal resolution (Y. Fang, Huang, et al., 2021; Z. Fang, Huang, et al., 2021; Mannino & Harvey, 2004; Q. Zhang, Zhou, et al., 2023). Consequently, it remains unclear how the removal or input of DBC varies temporally or across different estuaries. The challenges in elucidating the factors influencing DBC transport across estuaries stem from the complex sources and biogeochemical processes involved. The transport of chemicals in estuaries is closely related to particle concentration and salinity, both of which are strongly influenced by tidal dynamics and river discharge (Turner & Millward, 2002). Strong tidal currents facilitate sediment resuspension and elevate particle concentrations, while also influencing the release of porewater from sediments. Tidal patterns can exhibit both temporal variability (such as spring-neap and flood-ebb cycles) and spatial heterogeneity. Consequently, we hypothesize that the transport of DBC across estuaries will differ under varying hydrological conditions and among regions characterized by distinct tidal regimes.

To investigate the mechanisms governing DBC transport in estuarine environments, we conducted six field surveys across three different estuaries: the Jiulong River Estuary (JRE), the Changjiang Estuary (CJE), and the Pearl River Estuary (PRE), each exhibiting unique riverine discharges and tidal ranges. Published data from JRE and PRE were also collected for further analysis (Q. Zhang, Zhou, et al., 2023; Zhao et al., 2023). Moreover, laboratory simulation experiments (bio-degradation, photo-degradation and flocculation) were performed to elucidate the impact of different processes on DBC concentration. Furthermore, DBC concentrations in sediment porewater samples from the JRE and CJE were analyzed, and relevant models were employed to estimate DBC transport within the estuary. Our objectives are to (a) quantify the spatiotemporal variation in the changes in DBC concentration across estuaries and (b) elucidate the mechanisms that drive DBC transport across estuaries.

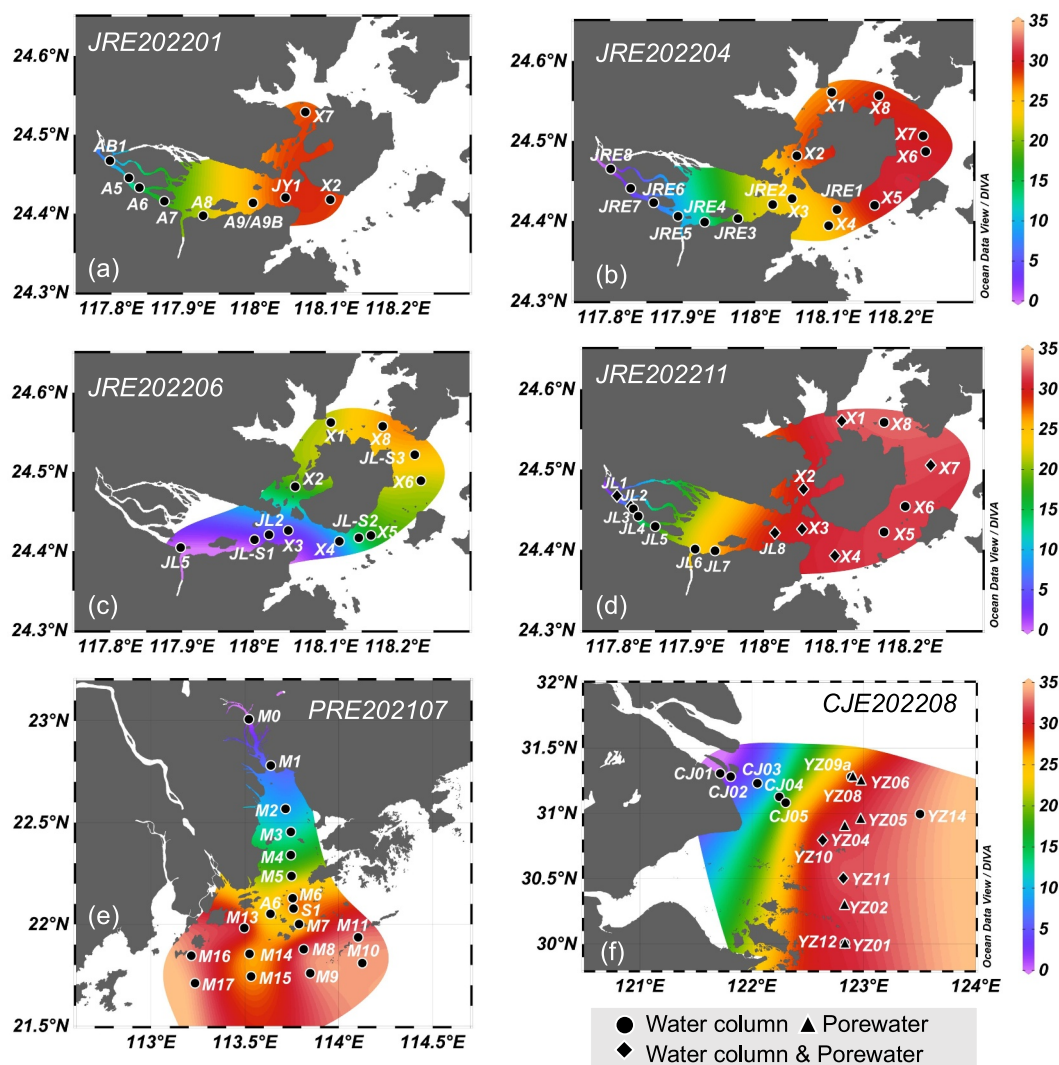


Figure 1. Sampling locations and surface layer salinity distribution across various estuaries. Panels (a–d) depict stations in the Jiulong River Estuary, while panels (e) and (f) represent stations in the Pearl River Estuary and Changjiang Estuary (CJE), respectively. Circles represent water column samples only, diamonds represent both water column and porewater samples, and triangles represent porewater samples only. The figures were generated using Ocean Data View software (Schlitzer, 2023).

2. Materials and Methods

2.1. Study Area

The three estuaries are predominantly situated in the subtropical regions along the eastern coast of China. The principal rivers feeding into the CJE, PRE, and JRE are the Changjiang, Pearl River (Zhujiang) and Jiulong River, respectively, with a drain basin area of 1.8, 0.45 and 0.014 Mkm² (sum of the two major tributaries, North Jiulong River and West Jiulong River). The mean river water discharges to CJE, PRE and JRE are 898, 283 and ~10 km³ yr⁻¹, respectively (Ministry of Water Resources of the People's Republic of China) (Figure 1). Therefore, these estuaries are categorized as major-, major-, and medium-river-affected estuaries, respectively.

The tidal patterns in these estuaries exhibit significant variability. The CJE experiences a regular semidiurnal tide with a mean tidal range of 2.0–3.1 m (Yang et al., 2001), while the JRE is predominantly influenced by semi-diurnal tides, exhibiting an average tidal range of 4.95 m (Wang et al., 2015). In contrast, the PRE is subject to a relatively weaker irregular semidiurnal tide, with a mean tidal range of 1.0–1.57 m (Table 1). The mean sampling areas in the CJE, PRE, and JRE were 23,500, 7,100, and 350 km², respectively.

Table 1
The Sampling Information, Including Hydrological Conditions, Tidal Range, and Mean Total Suspended Matter Concentration of the Six Sampling Campaigns From This Study and Three Sampling Campaigns From Literatures (Q. Zhang, Zhou, et al., 2023; Zhao et al., 2023)

Location	Sampling Date	Q (m ³ s ⁻¹)	Runoff (mm hr ⁻¹)	Tidal range (cm)	Mean TSM (mg L ⁻¹)
JRE	2022/1/18	62 ^a	0.016	496	53
JRE	2022/4/19	150	0.039	461	90
JRE	2022/6/18	2,827	0.74	436	76
JRE	2022/11/11	63 ^a	0.016	508	83
JRE	2014/7/22 ^b	297	0.078	326	28
JRE	2015/5/31 ^b	610	0.16	527	41
PRE	2021/07/19~21	4,700 ^c	0.038	163	25
PRE	2018/6/12~13 ^d	11,140 ^e	0.089	168	N.A.
CJE	2022/8/25	20,000 ^e	0.04	203	22

^aThe average value of 5 days before sampling due to the longer flushing time (~4–5 days) in the low discharge period (Du et al., 2024). ^bData from Zhao et al. (2023). ^cData source: <http://xxfb.mwr.cn/hydroSearch/greatRiver>. ^dData from Q. Zhang, Zhou, et al. (2023). ^eThe mean water discharge of August 2022 at Datong Station (Yangtze River Water Resources Commission of the Ministry of Water Resources, 2023).

2.2. Field Sampling and Sample Preparation

Sampling was conducted in August 2022 (summer) for the CJE, in January (winter), April (spring), June (summer), and November (autumn) 2022 for the JRE, and in July 2021 (summer) for the PRE (Figure 1). In the following text, the sampling campaign is marked as the location and sampling cruise, for example, JRE202204 means the April 2022 Jiulong River Estuary sampling (Figure 1). Daily water discharge during the sampling was recorded from <http://xxfb.mwr.cn/hydroSearch/greatRiver>, and the tidal range at the outlet location of each estuary was recorded from <https://www.chaoxibiao.net>.

Water samples were collected using a Conductivity-Temperature-Depth (CTD) instrument equipped with Niskin bottles (Seabird Scientific) for the PRE and CJE, while some surface samples from the JRE were collected using a polyethylene bucket (pre-cleaned with acid). Approximately 2 L of water was subsequently filtered through pre-weighed, and pre-combusted (4 hr at 400°C) 47 mm or 142 mm 0.7 μm GF/F filters by using a pump. The filtrates were then acidified to pH = 2 using HPLC-grade concentrated hydrochloric acid and stored in clean polycarbonate (PC) bottles (which had been soaked in 1N HCl for 12 hr and rinsed with ultrapure water) at 4°C. The filters were freeze-dried and re-weighed to determine the concentration of total suspended matter (TSM). Surface sediment samples (0–10 cm) from JRE and CJE were collected using a stainless steel grab and stored at –20°C.

Porewater samples were extracted through centrifugation of the surface sediment collected during the JRE202211 and CJE202208 sampling campaigns (Figure 1). Approximately 40–50 g of sediment samples were centrifuged at 2,500 rpm for 15 min in pre-cleaned centrifuge tubes, and the liquid supernatant was filtered through a 0.22 μm polyethersulfone (PES) filter. The filtrates were subsequently acidified to pH = 2 and extracted following the same protocol as other water samples.

For DBC analysis, ~1 L (containing ~100–200 μmol DOC) filtrate was concentrated using solid-phase extraction before DBC quantification (Dittmar et al., 2008). Briefly, the pH = 2 filtrates were passed through PPL cartridges (Agilent Technologies, 0.5 g/6 ml for JRE and PRE samples, 1 g/6 ml for CJE samples) at a flow rate of ~1 L hr⁻¹ for estuarine water samples driven by gravity. For porewater samples, since their volume was <20 ml (containing <200 μmol DOC), they were directly filled into the cartridge (500 mg/6 ml), and extracted in ~30 min. The cartridges were then dried with nitrogen gas, and then eluted with ~8 ml methanol. The eluent was designated as SPE-DOM and was stored at –20°C until further analysis.

The extraction efficiency of estuarine water samples was determined by evaporating the methanol of 100–200 μl eluent in an oven at 50°C and re-dissolved in pH = 2 HCl (HPLC-grade), and then determining the DOC concentration. The average extraction efficiency for water samples was 46 ± 12% (n = 44), close to previous reports for saline waters (Dittmar et al., 2008). The extraction efficiency for porewater samples was not determined.

Nevertheless, the samples loaded into the cartridges were within the recommended water volume and total amounts of DOC to avoid overload (Dittmar et al., 2008). Therefore, the concentration of DBC would not be affected.

2.3. Laboratory Incubation

Duplicate filtrates (through 0.7 mm GF/F filter) from the PRE at salinities of 0.3 were preserved in 2 L PC bottles and wrapped in aluminum foil at room temperature to assess the biodegradation of DBC. The filtrates contained in situ microbes; therefore, we did not add any extra inoculum. After 7 days, the filtrates were re-filtered to remove the influence of large size bacteria and acidified to pH = 2 for further analysis.

The flocculation simulation experiment was adapted from Khoo et al. (2022). Briefly, water samples from the upstream region of the JRE with a salinity of 0 were collected and filtered through a 142 mm 0.2 μm PC filter (Millipore). The filtrates were transferred to clean 500 ml PC bottles, and pre-combusted NaCl was added to adjust the salinity to 0, 3, 6, 12, and 30. Only NaCl was used to minimize potential contamination from organic carbon. Experiments were conducted in duplicates. A total of 10 PC bottles were placed on a shaking table for 2 hr, after which the samples were re-filtered using 47 mm 0.22 μm PES filters (Millipore) and subsequently acidified to pH = 2 for further analysis.

The photodegradation of the DBC experiment was conducted according to the method described by Stubbins et al. (2012). In summary, a water sample from Shidou reservoir near JRE (24.686°N, 118.012°E) was collected and then filtered through 0.22 μm filters (PES). Duplicate filtrates were placed into 2.5 L quartz flasks and treated with a saturated mercuric chloride solution (v:v, 1.5%) to inhibit microbial growth. The flasks were then sealed with polyethylene gloves and carefully positioned under natural sunlight for 16 days, with subsamples collected on days 1, 3, 5, 9, and 16 during July 2023 at Xiamen University. Running water was employed to maintain the temperature of the water samples below 38°C. The samples were subsequently transferred to 2L polycarbonate containers and acidified to a pH of 2. All acidified samples were stored at 4°C for further analysis.

2.4. Chemical Analysis

The concentration of DOC was measured using a total organic carbon (TOC) analyzer (Shimadzu TOC VCPH) at Xiamen University. To ensure the accuracy of the data, reference samples of deep seawater from the Sargasso Sea (obtained from Dr. D.A. Hansell's lab at the University of Miami, FL, USA) were used for verification. The average analytical error based on duplicate measurements was <10%.

DBC quantification was performed using the benzenepolycarboxylic acids (BPCAs) method following Dittmar (2008). Briefly, SPE-DOM containing 5–10 μmol C was oxidized for 9 hr with concentrated nitric acid at 170°C to release BPCAs. Following cooling, the solution was evaporated under nitrogen gas and then redissolved in phosphate buffer where it was stored frozen prior to analysis. The quantification of BPCAs was conducted using ultra-high performance liquid chromatography (UPLC) at the Third Institute of Oceanography, Ministry of Natural Resources, China. The concentration of DBC was calculated using a power function based on the two most robust BPCA monomers of benzenepentacarboxylic acid (B5) and benzenhexacarboxylic acid (B6) by the following equation (Stubbins et al., 2015):

$$\text{DBC} = 0.0891 \times (\text{B5} + \text{B6})^{0.9175} \quad (1)$$

The units for DBC, B5, and B6 were in μmol L⁻¹, nmol L⁻¹, and nmol L⁻¹, respectively. Calibration curves were inserted every 50–80 samples to monitor instrument performance. The standard deviation for duplicate and replicate analyses averaged less than 10%.

2.5. Models for Quantifying DBC Transport in Estuaries

A two-end-member mixing model was employed to evaluate the input and removal trends of DBC at specific salinities (Bao et al., 2023). The input or removal of DBC at a given location was calculated using the following formula:

$$\Delta\text{DBC} = \text{DBC}_{\text{obs.}} - \text{DBC}_{\text{theo.}} \quad (2)$$

Δ DBC represents the deviation between the observed DBC concentration ($DBC_{obs.}$) and the theoretical DBC concentration ($DBC_{theo.}$). The theoretical concentration, $DBC_{theo.}$, is derived from the linear mixing lines between riverine end-members (salinity < 1) and seawater end-members (Data set in Supporting Information S1, Bao et al., 2025). During two JRE cruises (JRE202201 and JRE202211), we were unable to collect samples with a salinity of 0 (<1) due to relatively low river discharge levels. Consequently, we utilized a discharge-weighted DBC concentration from the main tributaries sampled during a similar timeframe to represent the freshwater end-member (Data set 01 in Supporting Information S1, Bao et al., 2025). A positive value in Δ DBC indicates an input of DBC at a specific salinity, whereas a negative value indicates a removal of DBC.

The internal accumulation of DBC ($DBC_{int.}$, $\mu\text{mol C L}^{-1}$) can be estimated using the following equation:

$$DBC_{int.} = DBC_{eff.} - DBC_0 \quad (3)$$

where $DBC_{eff.}$ represents the effective concentration of DBC, and DBC_0 represents the freshwater DBC concentration. Two distinct models were employed to estimate $DBC_{eff.}$: a non-linear model and a linear model. The non-linear model utilized quadratic fitting for the input trend and exponential fitting for the removal trend between salinity and component concentration (García-Martín et al., 2021; Raymond & Bauer, 2001). The $DBC_{eff.}$ is estimated as the concentration of the constituent where the tangent at the seawater end-member intersects the y-intercept of the fitted equation; DBC_0 is calculated using the quadratic/exponential fitting line at salinity 0. In contrast, the linear model assumes that the component is conservatively well-mixed in samples with salinity > 15. Thus, the y-intercept of the linear regression line represents $DBC_{eff.}$, while DBC_0 is the DBC concentration at the lowest salinity (<1). Both models were employed in this study to highlight differences.

For the non-linear model, the maximum salinity varied across different sampling campaigns. To maintain consistency, we adopted a fixed salinity of 32 to represent the seawater end-member, following García-Martín et al. (2021) (Figure S1 in Supporting Information S1). Only regression coefficients (R^2) greater than 0.5 and fitting parameters that were statistically significant at $p < 0.05$ were utilized for further calculations (García-Martín et al., 2021). The non-linear models were further validated by comparing DBC_0 with measured freshwater samples, which showed no statistically significant difference (Student's t -test, $p > 0.05$). Moreover, the DBC concentration at salinity 32 estimated by our models was in close agreement with the measured values for salinities > 30 or slightly lower than the measured values at the highest salinity. For the linear model, only p -values less than 0.05 were considered statistically significant.

A positive $DBC_{int.}$ indicates input, while a negative value signifies removal (Zhao et al., 2023). The fraction of internal input or removal of DBC relative to riverine discharge was calculated by dividing $DBC_{int.}$ by DBC_0 ($DBC_{int.}/DBC_0$).

Additionally, the internal flux of DBC was estimated using the following equation:

$$F_{DBC_{int.}} = DBC_{int.} \times Q \quad (4)$$

Where $F_{DBC_{int.}}$ represents the internal flux of DBC (mol C s^{-1}) and Q denotes the riverine water discharge ($\text{m}^3 \text{s}^{-1}$).

2.6. Statistical Analysis

Linear, exponential and quadratic fittings were performed using R Studio (RCoreTeam, 2022). Student's t -test was performed to test the differences between the two groups in Microsoft Excel.

3. Results

3.1. Spatio-Temporal Variations in Physiochemical Parameters

In the JRE, river discharge rates measured during the sampling periods in January, April, June, and November were 62.5, 150, 2,827, and 63.2 $\text{m}^3 \text{s}^{-1}$, respectively. For the Changjiang and Pearl Rivers, the discharges into the CJE and PRE were approximately 20,000 and 4,700 $\text{m}^3 \text{s}^{-1}$, respectively (see Table 1). The year 2022 was notably dry in the Changjiang drainage basin, marking it as the most drought-affected year in the last 60 years. Our

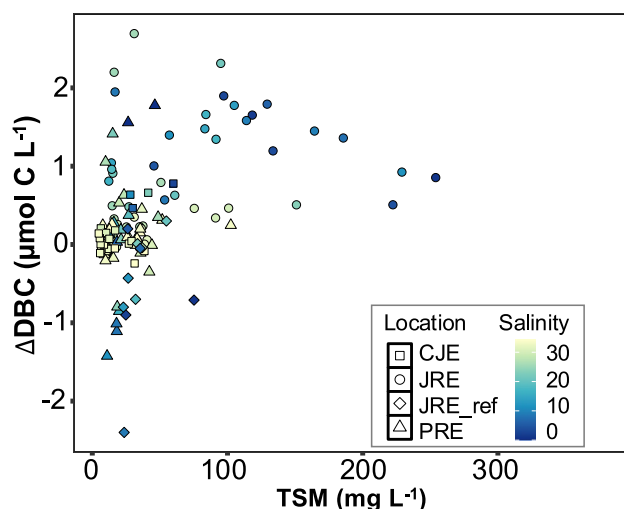


Figure 2. Distribution of total suspended matter and Δ DBC in relation to varying salinity levels. Different shapes represent distinct sampling locations, while JRE_ref denotes Jiulong River Estuary data sourced from the literature (Zhao et al., 2023).

sampling in the CJE coincided with this drought event (Duan et al., 2024). In August, the mean water discharge of approximately $20,000 \text{ m}^3 \text{ s}^{-1}$ was only one-third of the typical discharge for that time of year and was close to the low discharge level of approximately $12,000 \text{ m}^3 \text{ s}^{-1}$.

To facilitate comparisons among rivers, runoff was calculated by dividing water discharge by the basin area. The runoff values for the JRE were ~ 0.016 , 0.039, 1.0, and 0.016 mm hr^{-1} for January, April, June, and November, respectively. In contrast, the runoff for the Changjiang and Pearl Rivers was 0.04 and 0.038 mm hr^{-1} , respectively. The tidal ranges recorded during the January, April, June, and November samplings in the JRE were 4.96, 4.61, 4.36, and 5.08 m, respectively, while the tidal ranges for the CJE and PRE during their respective samplings were 2.03 and 1.63 m (refer to Table 1).

Salinity levels in all three estuaries ranged from 0 to approximately 30 during the six sampling campaigns, exhibiting an increase in salinity seaward (Figure 1). TSM concentrations varied from 5 to 60 mg L^{-1} in the CJE, from 9 to 377 mg L^{-1} in the JRE, and from 8 to 102 mg L^{-1} in the PRE (Figure 2). In the JRE, the highest mean TSM concentrations were recorded in April and June, whereas TSM concentrations in the CJE and PRE were significantly lower than those in the JRE (Table 1). Elevated TSM levels (greater than 100 mg L^{-1}) were primarily observed in the low to mid-regions of the JRE (Figure 2).

3.2. Spatio-Temporal Variations in DOC and DBC Concentrations

DOC concentrations ranged from 62 to $262 \text{ } \mu\text{mol L}^{-1}$ in the CJE during August 2022, and from 59 to $176 \text{ } \mu\text{mol L}^{-1}$ in the July 2021 sampling in the PRE. In the JRE, DOC concentrations varied from 100 to $213 \text{ } \mu\text{mol L}^{-1}$ in January, 83– $159 \text{ } \mu\text{mol L}^{-1}$ in April, 95– $130 \text{ } \mu\text{mol L}^{-1}$ in June, and 77– $174 \text{ } \mu\text{mol L}^{-1}$ in November. A significant negative correlation between DOC and salinity was observed across all sampling campaigns ($p < 0.05$ for all cases) (Figure S2 in Supporting Information S1).

DBC concentrations ranged from 0.86 to $7.4 \text{ } \mu\text{mol C L}^{-1}$ in the CJE during August and from 1.1 to $9.0 \text{ } \mu\text{mol C L}^{-1}$ in the PRE during July (Figures 3a and 3f). In the JRE, DBC concentrations varied from 2.5 to $6.3 \text{ } \mu\text{mol C L}^{-1}$ in January, 2.1– $6.6 \text{ } \mu\text{mol C L}^{-1}$ in April, 2.7– $6.1 \text{ } \mu\text{mol C L}^{-1}$ in June, and 2.0– $6.8 \text{ } \mu\text{mol C L}^{-1}$ in November (Figures 3b–3e). Throughout the six sampling campaigns, DBC concentrations were significantly negatively correlated with salinity. The B6/B5 ratio ranged from 0.22 to 0.28 in January, 0.22 to 0.25 in April, 0.24 to 0.26 in June, and 0.21 to 0.28 in November for samples from the JRE, while it ranged from 0.23 to 0.32 in the CJE and 0.22 to 0.28 in the PRE (Figure 4). Slightly elevated B6/B5 ratios were observed in the higher salinity regions of the JRE (Figure 4).

3.3. The Model Results for the Internal Input/Removal of DBC

Based on two end-member mixing models, DBC exhibited an input trend during all four cruises in the JRE and CJE, whereas a removal trend was observed in the PRE (Figure 3). The change in DBC (Δ DBC) ranged from -1.4 to $2.7 \text{ } \mu\text{mol C L}^{-1}$ across all sampling campaigns in this study (Figure 3 and Data set in Supporting Information S1, Bao et al., 2025). In most sampling campaigns, the input/removal trends were consistent throughout the estuary (Figure 3). Maximum input/removal rates in all three estuaries predominantly occurred in salinity regions of less than 15 (Figures 2 and 3).

In the majority of sampling campaigns, the non-linear model was significant. However, for the JRE202206 sampling, the R^2 value was 0.52, and both the quadratic and linear terms had p-values greater than 0.1, indicating insignificant regression. Consequently, the DBC_{eff} and DBC_{int} were not estimated from the non-linear model. The DBC_{eff} estimated by the non-linear model was 13.9, 9.9, and $12.6 \text{ } \mu\text{mol C L}^{-1}$ for JRE202201, JRE202204, and JRE202211, respectively, while it was 4.5 and $9.6 \text{ } \mu\text{mol C L}^{-1}$ for PRE202107 and CJE202208, respectively. The DBC_{eff} estimated for three previous sampling campaigns was $4.6 \text{ } \mu\text{mol C L}^{-1}$ for JRE201407 and $5.7 \text{ } \mu\text{mol C L}^{-1}$ for JRE201505, and $8.4 \text{ } \mu\text{mol C L}^{-1}$ for PRE201806. Accordingly, the DBC_{int} was 8.0, 3.8, and $5.9 \text{ } \mu\text{mol C L}^{-1}$.

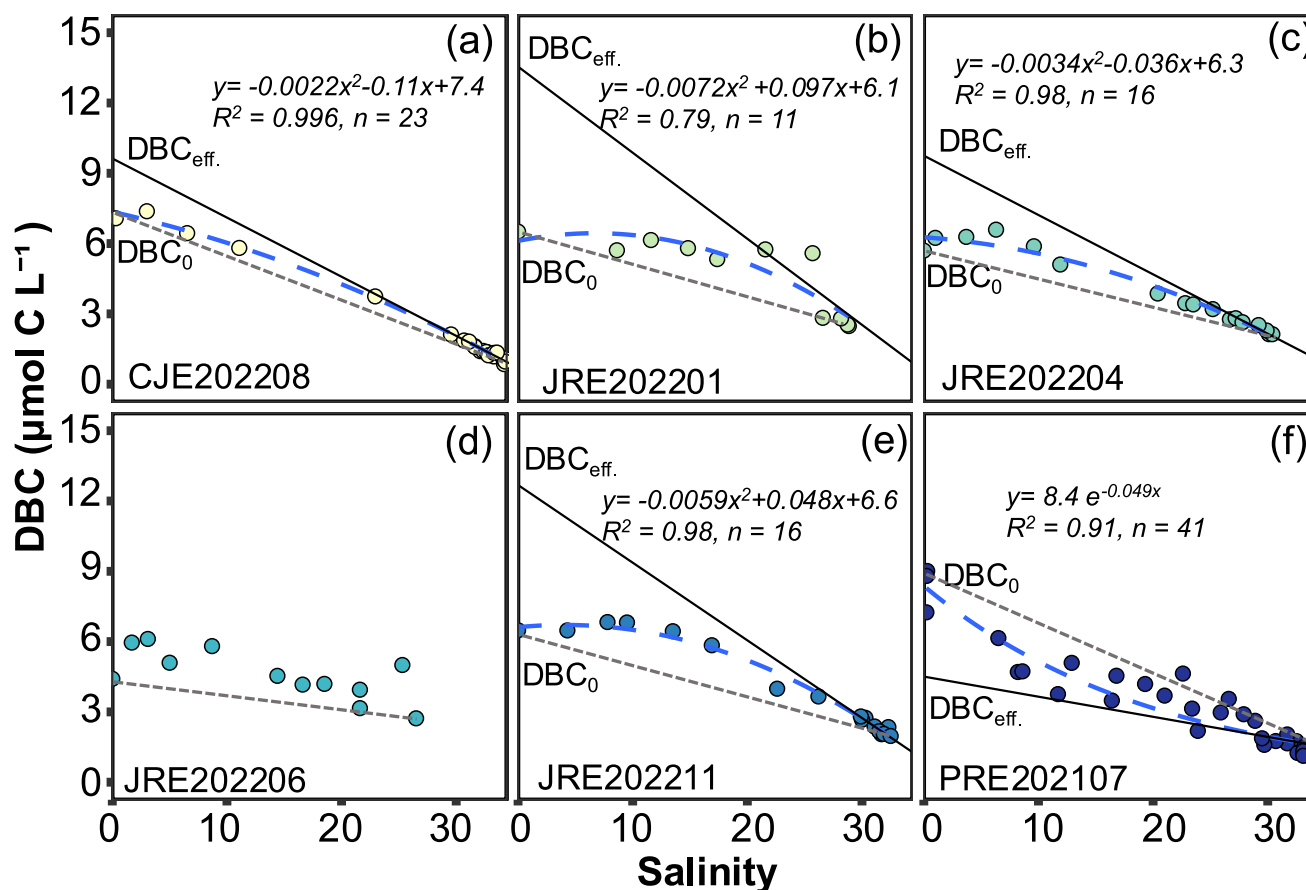


Figure 3. Relationship between dissolved black carbon (DBC) concentration and salinity in the studied estuaries. Panel (a) corresponds to the Changjiang Estuary (CJE); panels (b–e) represent the Jiulong River Estuary; and panel (f) illustrates the Pearl River Estuary. The blue dashed line indicates a quadratic or exponential regression between salinity and DBC concentration, the solid black line represents the tangent at the seawater end-member (fixed salinity of 32), and the dashed gray line signifies the conservative mixing line between freshwater and seawater. $DBC_{eff.}$ and DBC_0 refer to the effective and riverine concentrations of DBC, respectively.

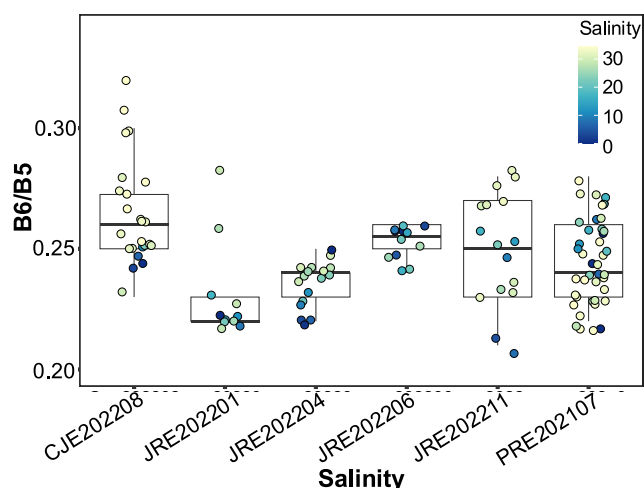


Figure 4. Distribution of the B6/B5 ratio in relation to salinity across various estuaries. The colors of the dots represent the salinity of the samples.

$C L^{-1}$ for JRE202201, JRE202204, and JRE202211, respectively, while it was $-3.9 \mu mol C L^{-1}$ for PRE202107 and $2.3 \mu mol C L^{-1}$ for CJE202208. Additionally, $DBC_{int.}$ for JRE201407 and JRE201505 was -1.4 and $-1.9 \mu mol C L^{-1}$, respectively. The estimation error of DBC_0 and $DBC_{eff.}$ was 1%–13% and 4%–24%, and for $DBC_{int.}$ was 7%–54% (Table 2).

In comparison to the non-linear model, the results from linear model revealed a similar trend but indicated lower $DBC_{eff.}$ and $DBC_{int.}$ values across all campaigns that met our model criteria (see Table S1 in Supporting Information S1). Specifically, the $DBC_{eff.}$ Ranged from 7.4 to 11 $\mu mol C L^{-1}$, while the $DBC_{int.}$ Ranged from 1.9 to 4.8 $\mu mol C L^{-1}$ during the three JRE 2022 sampling campaigns. Similarly, $DBC_{eff.}$ values for the PRE202107 and CJE202208 campaigns were estimated at 7.5 and 9.2 $\mu mol C L^{-1}$, respectively, resulting in $DBC_{int.}$ values of -0.86 and 2.1 $\mu mol C L^{-1}$. Due to limited sampling in regions with salinity greater than 15, $DBC_{eff.}$ and $DBC_{int.}$ values for the JRE201407 and JRE201505 campaigns could not be calculated. However, the $DBC_{eff.}$ and $DBC_{int.}$ for PRE201806 were determined to be 5.3 and 1.1 $\mu mol C L^{-1}$, respectively (see Table S1 in Supporting Information S1).

The $F_{DBC_{int.}}$ varied from 0.37 to 46 $mol C s^{-1}$ in campaigns exhibiting input trends, while it ranged from -18 to $-0.42 mol s^{-1}$ in campaigns characterized by removal trends, as estimated by the non-linear model. The $F_{DBC_{int.}}$ values

Table 2
The Estimated Internal Input/Removal of Dissolved Black Carbon for Different Cruises

Sampling campaign	DBC ₀ (μmol C L ⁻¹)	DBC _{eff.} (μmol L ⁻¹)	DBC _{int.} (μmol C L ⁻¹)	DBC _{int.} /DBC ₀ (%)	F _{DBC_0} (mol C s ⁻¹)	F _{DBC_int.} (mol C s ⁻¹)
JRE202201	5.9 ± 0.78	13.9 ± 3.4	8.0 ± 3.3	123	0.37 ± 0.049	0.50 ± 0.20
JRE202204	6.2 ± 0.20	9.9 ± 1.1	3.8 ± 1.1	57	0.93 ± 0.030	0.56 ± 0.17
JRE202206	5.2	N.A.	N.A.	N.A.	14.7	N.A.
JRE202211	6.7 ± 0.21	12.6 ± 0.81	5.9 ± 0.79	91	0.42 ± 0.013	0.37 ± 0.050
JRE201407 ^a	6.0 ± 0.66	4.6 ± 0.88	-1.4 ± 0.73	-32	1.8 ± 0.20	-0.42 ± 0.22
JRE201505 ^a	7.6 ± 0.21	5.7 ± 0.26	-1.9 ± 0.22	-25	4.6 ± 0.13	-1.2 ± 0.13
PRE202107	8.4 ± 0.32	4.5 ± 0.28	-3.9 ± 0.26	-49	39 ± 1.5	-18 ± 1.2
PRE201806 ^b	5.5 ± 0.52	8.4 ± 1.6	2.8 ± 1.5	53	61 ± 5.8	31 ± 17
CJE202208	7.3 ± 0.10	9.6 ± 0.43	2.3 ± 0.42	30	148 ± 2.0	46 ± 8.4

Note. N.A.: Not available. ± represent the propagated error from the quadratic or exponential simulation. ^aData were calculated from Zhao et al. (2023). ^bData were calculated from Zhang, Zhou, et al. (2023).

estimated by the linear model were found to be 20%–100% of those estimated by the non-linear model (see Table 2, Table S1 in Supporting Information S1).

3.4. DBC in Estuarine Sediment Porewater

The concentration of DBC in porewater from the JRE ranged from 6.9 to 22 μmol C L⁻¹ across a salinity range of bottom water from 4.8 to 31.8 (Figure 1 and Table 3), with higher concentrations observed in the upper reaches of the JRE. In contrast, porewater concentrations in the CJE ranged from 4.8 to 11 μmol C L⁻¹, where salinity levels

Table 3
Locations, Concentrations and B6/B5 Ratio of Dissolved Black Carbon in Porewater Samples Collected in Jiulong River Estuary and Changjiang Estuary

Region	Station	Latitude (°N)	Longitude (°E)	Water depth (m)	Porewater_DBC (μmol C L ⁻¹)	B6/B5
JRE202211	X1	24.56	118.11	4.4	8.5	0.93
	X2	24.48	118.05	4.2	6.9	0.63
	X3	24.43	118.05	11.5	13	0.78
	X4	24.39	118.10	10.4	14	0.69
	X7	24.51	118.23	16.9	8.9	0.70
	JL1	24.47	117.80	3.9	16	0.77
	JL2	24.45	117.82	5.6	15	0.28
	JL8	24.42	118.01	12.5	22	0.28
Mean					13	0.63
sd ^a					5.0	0.23
CJE202208	YZ01	30.00	122.83	47	4.8	0.86
	YZ02	30.30	122.83	30.4	7.4	0.79
	YZ04	30.90	122.83	27.7	8.9	0.86
	YZ05	30.96	122.97	47.6	11	1.06
	YZ06	31.25	122.98	60.8	11	1.07
	YZ08	31.28	122.90	64.9	9.4	0.97
	YZ10	30.79	122.63	27.9	5.8	0.80
	YZ11	30.50	122.82	42.6	8.1	1.03
Mean					8.3	0.93
sd ^a					2.3	0.12

^aStandard deviation.

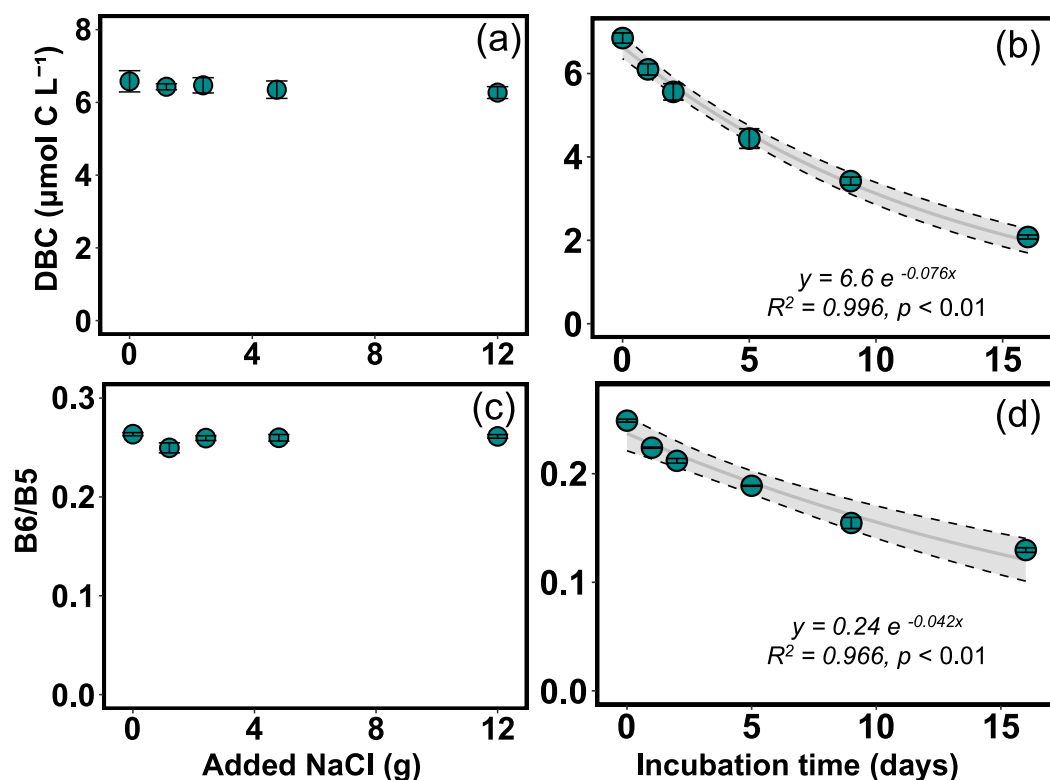


Figure 5. Variation in dissolved black carbon concentration and the B6/B5 ratio during laboratory simulations. Panels (a, c) depict flocculation; and panels (b, d) represent photodegradation. The x-axis in panels (a, c) indicates the mass of NaCl added to 400 mL of Milli-Q water in a 500 mL polycarbonate bottle. Error bars denote the standard deviation from duplicate samples, which were smaller than the size of the circles in the flocculation and photodegradation experiments.

exceeded 32. The B6/B5 ratio in the JRE porewater samples varied from 0.28 to 0.93, while in the CJE samples, it ranged from 0.79 to 1.1. Notably, lower B6/B5 ratios were recorded in the upper estuarine region of the JRE (see Table 3), although all values were generally higher than those observed in water column samples, which ranged from 0.20 to 0.35.

3.5. Changes of DBC During Laboratory Simulation

Following the addition of varying proportions of NaCl (0, 1.2, 2.4, 4.8, and 12 g), the DBC concentration fluctuated between 6.6 ± 0.3 (initial concentration) and $6.3 \pm 0.2 \mu\text{mol C L}^{-1}$ (see Figure 5a). The B6/B5 ratio was observed to range from 0.25 ± 0.005 to 0.26 ± 0.002 (see Figure 5c). Over a 7-day bio-incubation period, the change in DBC concentration was less than $0.1 \mu\text{mol L}^{-1}$ (<2% of the initial concentration) (Table S2 in Supporting Information S1), while B6/B5 values did not show any change (Table S2 in Supporting Information S1).

During the photodegradation, the DBC concentration decreased continuously from 6.9 ± 0.12 to $2.1 \pm 0.05 \mu\text{mol C L}^{-1}$, representing a reduction of 70% from day 0 to day 16 (see Figure 5b). Correspondingly, the B6/B5 ratio declined from 0.25 ± 0.001 to 0.13 ± 0.002 (see Figure 5d). The degradation rate of DBC was calculated to be -0.076 d^{-1} ($R^2 = 0.996$, $n = 6$).

4. Discussion

4.1. Seasonal and Regional Variations in the Transport of DBC Across Estuaries

The significant negative correlations observed between DOC or DBC concentrations and salinity ($p < 0.05$ for all comparisons, data not shown) across all sampling campaigns indicate that the physical mixing of saline and freshwater is the primary factor influencing the distribution of DOC and DBC in the estuary. This finding is consistent with previous research conducted in coastal seas and other estuarine environments (Bao et al., 2023; Y.

Fang, Huang, et al., 2021; Fang et al., 2017; Q. Zhang, Zhou, et al., 2023). The riverine DBC concentration (DBC_0) exhibited relative stability in the JRE across different sampling campaigns, which aligns with our earlier annual observations in the lower reach of the Jiulong River (Bao et al., 2019). During the June 2022 sampling campaign (JRE202206) (Figure 3), the slightly lower concentration coincided with a discharge nearly 10 times the annual mean. This pattern aligns with our earlier observations from the 2014–2015 extreme rainfall events, which were attributed to dilution effects (Bao et al., 2019).

Although the effective DBC (DBC_{eff}) estimated by the two models differed, the trends regarding input or removal, as well as the absolute values of DBC_{eff} , were generally consistent across most sampling campaigns (Table 2). This consistency allows for a discussion of the potential mechanisms driving their spatiotemporal trends. In the non-linear model, both DBC_{eff} and DBC_0 were determined by regression analysis of the entire data set, while in the linear model, DBC_0 was defined by the samples taken at zero salinity, which may have been influenced by random effects. Furthermore, in some sampling campaigns, there were insufficient samples with salinity greater than 15 for accurate estimation of DBC_{eff} . Consequently, we primarily focused on the results derived from the non-linear model. Compared to DBC_0 , DBC_{eff} exhibited a twofold difference in the JRE, indicating that estuarine sources and processes played significant roles in the efflux of DBC from estuaries (Bao et al., 2023; Z. Fang, Huang, et al., 2021; Mannino & Harvey, 2004; Q. Zhang, Zhou, et al., 2023; Zhao et al., 2023). This is particularly evident given that the magnitude of DBC removal and input may exceed 50% of riverine discharge (Table 2).

Our findings indicate that both input and removal trends can occur within the same estuary at different times or across different estuaries. For example, in the JRE, a removal trend was documented in two previous cruises (Zhao et al., 2023), whereas input trends were observed during the four sampling campaigns conducted in this study (Figure 3). Similarly, in the PRE, removal of approximately 50% (around $4.0 \mu\text{mol C L}^{-1}$) was noted in our study (Table 2), contrasting with a documented input trend in another investigation (Q. Zhang, Zhou, et al., 2023). These results suggest that DBC input and removal are not site-specific phenomena.

Hydrological conditions are also critical as they influence flushing times and dynamic processes within estuarine environments. However, the differences in runoff between input and removal trends were found to be statistically insignificant (t -test, $p > 0.05$), irrespective of whether extreme rainfall events were included or excluded. This suggests that hydrological conditions are not the primary influencing factors. Nevertheless, in the JRE, the concentration of DBC tends to decrease, and the ratio of DBC_{int}/DBC_0 approaches 0 at higher water discharge levels (Table 2). This observation implies that DBC may bypass the estuarine region. This pattern is analogous to the behavior of DOC, which, under elevated discharge conditions, tends to be conservatively mixed and is attributed to shorter flushing times (Raymond & Bauer, 2001).

Tidal dynamics, including the tidal range across estuaries and the spring-neap and flood-ebb tidal cycles within a single estuary, are also critical variables. Both input and removal trends were observed under low (<2 m) and high (>3 m) tidal range conditions, indicating that tidal range does not serve as a determinant of the observed input/removal patterns. Additionally, DBC input and removal were recorded in the same estuary (JRE) during both spring and neap tides (Table 1), ruling out the influence of the spring-neap tidal cycle. Notably, all removal trends were observed during ebb tides, while input trends were recorded during flood tides across three different estuaries (Figure 6). These patterns suggest that processes occurring during flood-ebb cycles significantly influence the net input and removal of DBC in estuarine environments.

4.2. Potential Mechanisms Driving the Input and Removal of DBC in Different Estuaries

To elucidate the mechanisms underlying the input and removal of DBC, it is essential to understand the processes and sources that influence DBC transport across estuaries. Flushing time is a critical parameter for assessing the extent to which various processes affect the cycling of dissolved organic matter (DOM). Flushing time is typically estimated by considering riverine discharge, tidal influences, and the distribution of saline water (Du et al., 2024; Liu et al., 2018). Based on previous estimations in the same estuaries (JRE, PRE, CJE), we estimated that flushing time was less than 1 day in JRE samples from June 2022, approximately 2 days in JRE samples from July 2014, and May 2015, and around 6 days in JRE samples from January, April, and November 2022. Flushing times were estimated to be approximately 2–5 days in PRE and ~5 days in CJE during sampling campaigns from this and previous studies (see estimation method in Text S1 in Supporting Information S1).

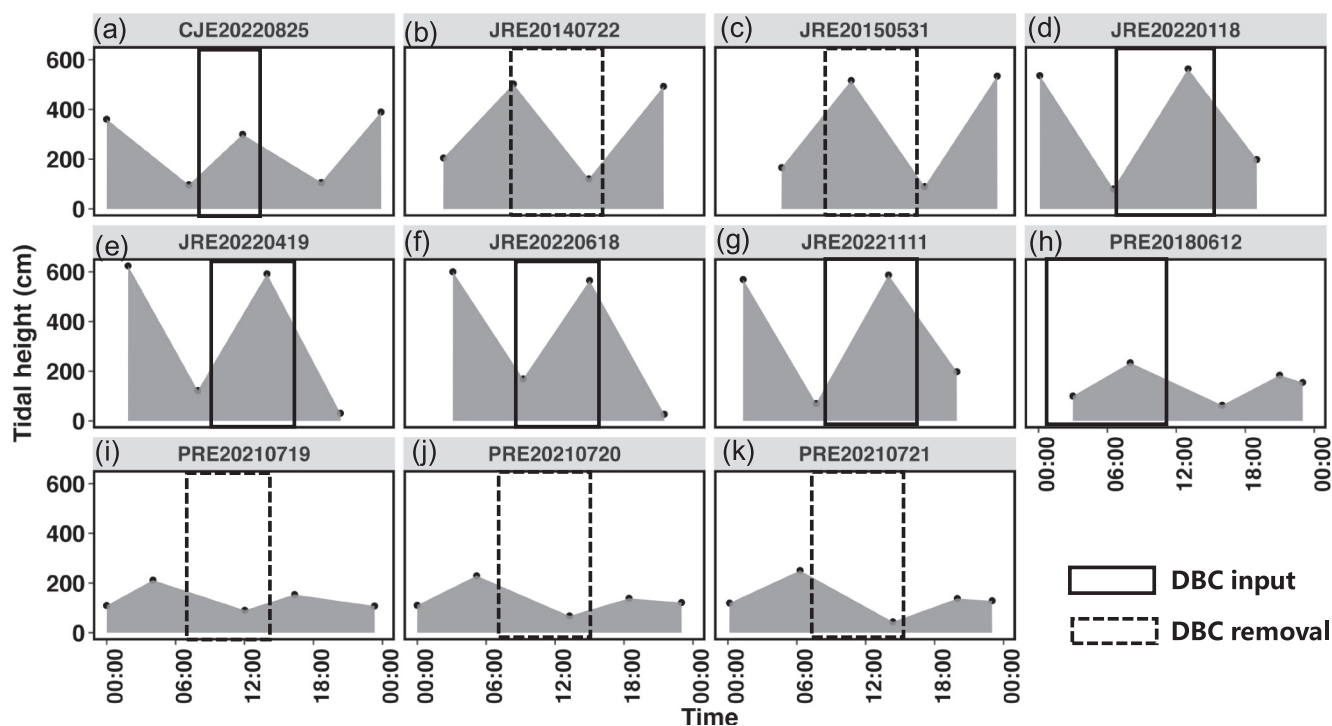


Figure 6. Relationship between flood/ebb tides and the input/removal of dissolved black carbon in the studied estuaries. Panel (a) depicts the Changjiang Estuary (CJE); panels (b–g) represent the Jiulong River Estuary (JRE); and panels (h–k) illustrate the Pearl River Estuary (PRE). The exact time of each station in JRE201407 and JRE201505 were not available, but were all collected during day time (8:00 to 16:00), as shown in panels (b, c). The sampling time for PRE201806 was from Q. Zhang, Zhou, et al. (2023).

4.2.1. Processes Removing DBC From Estuaries

DBC removal can occur through various mechanisms, including flocculation, photodegradation, and particle sorption (Coppola et al., 2014; Z. Fang, Huang, et al., 2021; Stubbins et al., 2012). Biodegradation of DBC appears to be negligible, as demonstrated by both our bio-incubation experiment (Table S2 in Supporting Information S1) and a previous study (Bostick et al., 2021). Photochemical degradation was found to be effective in removing DBC in our experiments (Figure 5) and in a previous study (Stubbins et al., 2012). However, considering flushing time, water depth, and UV attenuation in the water column (Huovinen et al., 2003) (see Text S2 in Supporting Information S1 for calculation method), we estimated that photodegradation would account for less than 2% of DBC removal in all three estuaries, indicating that it is a minor factor. Furthermore, the highest DBC removal occurred in the bottom layer of PRE, further excluding photodegradation as the primary mechanism for DBC removal. Photodegradation has been deemed negligible in removing terrestrial phenolic compounds in fluvial systems due to interference from suspended particles (Ward et al., 2013).

Flocculation is a prevalent process in estuarine environments where freshwater interacts with seawater. Our laboratory experiments demonstrated that variations in salinity alone could result in a maximum removal of DBC of $0.3 \mu\text{mol C L}^{-1}$, which corresponds to approximately 5% of the riverine DBC concentration in the JRE within 2 hours. Although this change is within the range of analytical error, the magnitude of DBC removal via flocculation is consistent with previous studies reporting bulk DOC removal of approximately 3% and colored dissolved organic matter (CDOM) removal averaging around 5% in other regions (Khoo et al., 2022; Uher et al., 2001). It is important to note that laboratory results may not fully replicate in situ conditions, where factors such as microbial exudates may enhance flocculation (Eisma, 1986; Manning et al., 2010). Nevertheless, flocculation alone could not account for the 10%–50% DBC removal observed in our study (Table 2).

In addition to flocculation, particle sorption is also proposed to be a rapid process that can occur within hours and is recognized as a significant mechanism in removing DBC and CDOM in the estuarine and open ocean (Coppola et al., 2014; Uher et al., 2001; Yamashita et al., 2022). The highest removal rates were observed at TSM

concentrations of 10–30 mg L⁻¹. This may be partly attributed to the tendency of lower particle concentrations to adsorb DBC while simultaneously promoting its photodegradation.

4.2.2. Potential Processes/Sources Contributing to DBC Input

The positive internal fluxes of DBC observed across all estuaries indicate the presence of additional sources that are likely common to estuarine regions. Potential sources include atmospheric deposition, photo-dissolution from the particulate phase, contributions from coastal wetlands, and SGD (Bao et al., 2023; Roebuck et al., 2017; R. Zhang, Zhou, et al., 2023). Our previous research estimated that atmospheric deposition could account for approximately 3% of the annual riverine discharge of DBC to the JRE (Bao et al., 2022; R. Zhang, Zhou, et al., 2023; Zhao et al., 2023). Due to the influence of the East Asian Monsoon, atmospheric deposition of DBC was significantly higher during winter and spring when riverine discharge was low (Table 1), making it a more critical factor for DBC levels in the estuarine region.

Distinguishing between the processes of photo-dissolution and the desorption of DBC from particles is challenging as both are associated with the particulate phase. A previous study observed an increase in DBC levels in the river during the rainy season, which was attributed to desorption from particles (Marques et al., 2017). However, Roebuck et al. (2017) reported that the dissolution of DBC was enhanced by approximately threefold under light exposure, suggesting that light-induced dissolution was a significant mechanism for DBC production. Like photodegradation, photo-dissolution occurs primarily in the surface layer. Considering the photo-dissolution rates reported by Roebuck et al. (2017), along with flushing times and soil organic carbon content in the estuarine water column (Huang & Yu, 2017; Qiao et al., 2019; Wu et al., 2015; Yu et al., 2010), we estimated that the input of DBC due to photo-dissolution averaged less than 0.05 μmol C L⁻¹ (Text S3 in Supporting Information S1). In contrast, desorption can occur throughout the entire water column. Mannino and Harvey (2004) also noted that the maximum input of DBC occurred in turbid zones, attributing it to desorption from particles. However, quantitative contributions remain unclear and warrant further investigation.

SGD has been recognized as a previously overlooked contributor to the release of substances into the oceans (Moore, 2010). We adopted a widely accepted definition of SGD, which encompassed all water flow along continental margins from the seabed to the coastal sea, with scale lengths ranging from meters to kilometers, irrespective of fluid composition or driving mechanisms (Moore, 2010). Our definition of SGD includes both freshwater discharge and recirculated seawater. Previous estimates of SGD flux in the three studied estuaries utilized radioisotopes ²²⁶Ra and ²²⁸Ra, indicating that recirculated seawater is the predominant source of SGD (Du et al., 2024; Guo et al., 2020; Liu et al., 2018). Based on these studies, we estimated that the SGD flux corresponded to approximately 12% of riverine discharge in the JRE, and 15% in both the PRE and CJE under the freshwater discharge levels observed in our study (Text S4 in Supporting Information S1) (Du et al., 2024; Gu et al., 2012; Liu et al., 2018; Q. Zhang, Zhou, et al., 2023; Zhao et al., 2023).

Limited information exists regarding the concentration of DBC in recirculated seawater. Sediment porewater may contribute to SGD. Prior studies measured DBC concentrations in porewater from the intertidal beach of Spiekeroog Island, which ranged from 7 to 280 μmol C L⁻¹ (Seidel et al., 2014, 2015), with concentrations increasing with sediment depth. The DBC concentration in our porewater samples (range: 5–22 μmol L⁻¹, mean ± standard deviation: 11 ± 4.4 μmol C L⁻¹, *n* = 16, Table 3) was consistent with these earlier measurements and exhibited enrichment in DBC compared to the overlying water column (2–9 times that of the water column or bottom water, Table S2 in Supporting Information S1), suggesting that the recirculation process served as a source of DBC to the estuarine environment. Given that we only sampled the surface sediment (depth < 5 cm), this concentration should be considered a lower estimate of the DBC concentration in SGD.

The elevated DBC concentrations observed in sediment porewater within estuaries remain enigmatic, particularly as no direct combustion occurs within porewater. Potential mechanisms for the release of DBC from iron oxides/hydroxides in sediments under anoxic conditions (Coppola et al., 2014; Kaiser & Guggenberger, 2000; Seidel et al., 2015) and/or production via Fenton reactions (Chen et al., 2014; Goranov et al., 2024) may account for this phenomenon. The higher B6/B5 ratio observed in porewater DBC compared to the overlying water may be attributed to the preferential desorption of more condensed aromatic black carbon (e.g., 0.28–1.1 vs. 0.21–0.27).

The SGD flux of DBC ($F_{\text{DBC-SGD}}$) can be estimated by multiplying the DBC concentration in SGD (DBC_{SGD} , μmol C L⁻¹) by the SGD flux (F_{SGD} , in m³ s⁻¹).

$$F_{\text{DBC_SGD}} = \text{DBC}_{\text{SGD}} \times F_{\text{SGD}} \quad (5)$$

Here, $F_{\text{DBC_SGD}}$ represents the mean values during the flushing period, which encompassed 1–6 flood-ebb tidal cycles. To avoid overestimating SGD flux, the DBC concentration in the saline SGD end-member is defined as the difference between sediment porewater and seawater in each estuary (Cabral et al., 2023). Assuming that the DBC concentration in recirculated SGD remains consistent across different seasons, we estimated that $F_{\text{DBC_SGD}}$ ranged from 0.06 to 18 mol C s⁻¹ (Table S3 in Supporting Information S1), accounting for approximately 13%–47% of the observed $F_{\text{DBC_int.}}$ during the sampling periods coinciding with flood tides. These findings indicate that SGD constitutes a significant source of DBC in the estuarine region. Due to the higher B6/B5 ratio in porewater (Table 3), an increase in this ratio would be expected given the significant contribution of SGD to DBC. However, such an increase was not clearly observed in our study. This could be attributed to the simultaneous occurrence of multiple processes that influence the B6/B5 ratio in different ways, thereby complicating its use as a reliable tracer for identifying DBC sources in the estuarine region.

In addition to SGD from the seabed, coastal wetlands, such as salt marshes and mangroves, also contribute significant amounts of DBC to estuarine and coastal regions (Ding et al., 2014; Dittmar et al., 2012). However, this water flux has already been accounted for in the SGD estimates, as the contribution from wetlands is primarily driven by the recirculation of seawater, making it indistinguishable from SGD flux when measured using radioisotopes.

4.2.3. Hypothesis for the Observed Flood-Ebb-Related Input-Removal Pattern of DBC

The observed input and removal of DBC reflect the net effect of biogeochemical processes and sources. The removal patterns observed during ebb tides suggest enhanced DBC removal, while the input trends during flood tides may indicate contributions from additional sources. Based on our estimations, the contributions of flocculation, photodegradation, and biodegradation to DBC removal appear negligible, suggesting that sorption may play a significant role. However, the quantitative impact of the sorption process remains to be confirmed in future studies. Additionally, the input of DBC via photo-dissolution was minimal, and atmospheric deposition showed no correlation with tidal patterns, thereby excluding these factors as major contributors to the observed input patterns.

As previously mentioned, SGD is a significant source of DBC. Du et al. (2024) monitored SGD flux in the JRE at a fixed site during a flood-ebb tidal cycle and found that it decreased to less than 20% (and in some instances close to 0%) of the flux observed during flood tides. It has been suggested that during ebb tides, the lower and more intense pycnocline acts as a barrier, limiting particle resuspension (Scully & Friedrichs, 2003), and consequently reducing SGD flux. In contrast, during flood tides, sediments can be resuspended higher in the water column, facilitating SGD flux and enhancing the mixing of SGD into the upper water column. The mean TSM concentration was approximately three times higher during flood tide sampling campaigns compared to ebb tides under similar hydrological conditions in the JRE, which may reflect tidal influences (Table 1). Due to its significance, the differences in SGD flux during the flood-ebb tidal cycle could potentially affect the observed input and removal patterns. Furthermore, changes in TSM resulting from flood-ebb tidal cycles may also influence sorption and desorption processes in the water column, thereby further affecting DBC input and removal.

4.3. Quantitative Estimation of the Internal Flux of DBC

The varying trends of DBC input and removal observed in this study suggest that, when considering the internal flux and removal of substances during estuarine transport, it is essential to account for the entire flood-ebb tidal cycle. A previous investigation in the York River Estuary found that the internal accumulation of DOC was negatively correlated with riverine water discharge, a phenomenon attributed to reduced flushing time (accumulation time) during periods of higher discharge (Raymond & Bauer, 2001). In this study, we observed that the internally derived DBC ($\text{DBC}_{\text{int.}}$) from the non-linear model exhibited an exponential relationship with the reciprocal of runoff (1/Runoff (hr mm⁻¹)), reflecting flushing time (Moore et al., 2006) during campaigns that recorded input trends ($R^2 = 0.83$, $n = 5$, $p < 0.05$, Figure S3 in Supporting Information S1), thereby indicating the influence of flushing time on DBC accumulation. Due to the limited number of sampling campaigns that recorded removal trends, establishing a robust relationship between $\text{DBC}_{\text{int.}}$ and runoff proved challenging. Nonetheless,

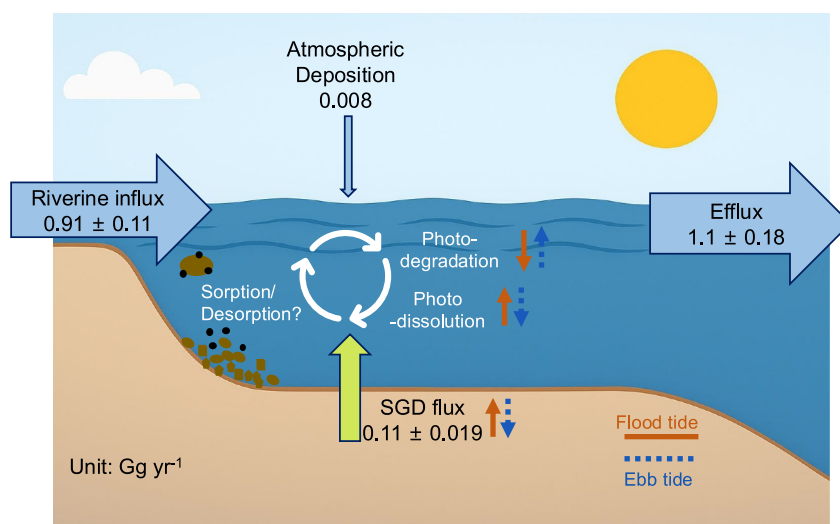


Figure 7. A conceptual diagram illustrating the transport of dissolved black carbon driven by the flood-ebb tidal cycle in the estuarine region. The blue and red arrows denote changes occurring during flood and ebb tides, respectively, while the up and down arrows indicate enhancement or inhibition of the process. The numbers represent the flux of various terms in the Julong River Estuary.

the absolute $DBC_{int.}$ values were higher during periods of lower runoff in the PRE campaign compared to those in the JRE201407 and JRE201505 campaigns, underscoring the impact of flushing time.

Since the JRE sampling encompassed the entire hydrograph, it allowed for further estimation of DBC transport across the estuary. Although the input and removal trends varied under different hydrological conditions, the effective DBC ($DBC_{eff.}$) and initial DBC (DBC_0) values remained relatively consistent across both high (JRE201407 and JRE201505) and low discharge levels (JRE202201, JRE202204, and JRE202211). Based on the distribution of daily water discharge and assuming similar $DBC_{eff.}$ and DBC_0 values under high (greater than annual mean discharge) and low (less than annual mean discharge) conditions (Table S4 in Supporting Information S1), we estimated that the riverine discharge of DBC to the estuary was 0.91 ± 0.11 Gg yr⁻¹ (Figure 7), while the DBC exported from the estuary was 1.1 ± 0.18 Gg yr⁻¹. The \pm values for these two fluxes represent the standard deviations in $DBC_{eff.}$ and DBC_0 . Additionally, the annual SGD flux was reported to be approximately $10 \pm 1.7\%$ of river discharge, which was about 1.1 ± 0.17 km³ yr⁻¹ (Du et al., 2024). Multiplying this SGD volume by the DBC concentration in SGD (8.6 ± 0.48 $\mu\text{mol C L}^{-1}$), we estimated the DBC flux from SGD (F_{DBC_SGD}) to be 0.11 ± 0.019 Gg yr⁻¹. This SGD flux represents a lower estimate, as it pertains only to the SGD flux in the mixing area (area: 71 km²), while our sampling encompassed a mean estuarine area of approximately 350 km². The wet and dry atmospheric deposition was estimated to be around 0.024 t km⁻² (Bao et al., 2022; R. Zhang, Zhou, et al., 2023). By multiplying this deposition rate by the estuary area (350 km²), we calculated the atmospheric deposition to be 0.008 Gg yr⁻¹ (Figure 7). Our estimations indicate a mass balance between input and output, highlighting that the estuarine SGD flux could reach approximately 12% of the riverine DBC flux in the JRE, representing a previously overlooked source of DBC to the ocean.

4.4. Limitations and Implications

Although three representative temperate and subtropical estuaries were examined in this study, certain limitations must be acknowledged. The observed patterns should not be generalized to other components of DOM, particularly the bio-labile fraction. Due to its relative resistance to biodegradation, DBC transport across estuaries is predominantly influenced by physical processes such as flocculation and source inputs. In areas with extended flushing times, biological processes may gain significance, further influencing DOM transport within the estuaries. Moreover, the observed patterns may not apply to regions characterized by strong flocculation, which is frequently observed in areas with elevated DOC concentrations, such as boreal systems (Z. Fang, Huang, et al., 2021; Khoo et al., 2022). Nonetheless, to our knowledge, this study encompasses the most sampling campaigns related to DBC transport across estuaries. Although it remains uncertain whether the identified flood-ebb pattern applies to other

estuaries, our findings highlight the necessity of considering the entire tidal cycle when estimating the internal flux of terrestrial DOM from estuaries.

The current mass balance of DBC indicates the presence of “unknown” sources of DBC in the ocean. Our study suggests that SGD is a significant yet largely underappreciated source. In our research, the SGD flux of DBC represented approximately 12% of the riverine discharge of DBC, making it the second-largest known source of DBC in the JRE. On a global scale, the recirculated SGD flux of water is estimated to be approximately 125% of the riverine discharge (around $45 \times 10^{12} \text{ m}^3 \text{ yr}^{-1}$) (Du et al., 2024; Moore et al., 2008; Raymond & Spencer, 2015). By multiplying the mean SGD end-member DBC concentration (excluding DBC in the estuarine region, approximately $8 \mu\text{mol C L}^{-1}$) by the SGD flux, we estimate that SGD could contribute approximately 4.3 Tg yr^{-1} of DBC to the ocean, which corresponds to about 16%–23% of the global riverine discharge (Jaffé et al., 2013; Jones et al., 2020). During the recirculation of seawater, it remains unclear whether there is fractionation of stable carbon isotopes in DBC. A recent study utilizing the thermo-oxidation method to analyze DBC isotopes in sediment porewater from the East China Sea found a significantly enriched stable carbon isotope signal (Fu et al., 2023), suggesting the potential of SGD flux as a primary source of DBC in the ocean. Future research should focus more on the SGD of DBC in various regions, including its stable carbon isotopic composition, to enhance our understanding of DBC cycling in the ocean.

5. Conclusions

To investigate the cycling of DBC in estuarine regions, we conducted six sampling campaigns across three estuaries and supplemented our findings with data from previous studies. Our results indicated that DBC exhibited both input and removal trends, which varied among different estuaries as well as within the same estuary. These trends were not correlated with riverine discharge levels, tidal ranges, or geographic locations; rather, they were associated with flood-ebb tidal cycles. Specifically, the input of DBC predominantly occurred during flood tides, while its removal was primarily observed during ebb tides. Considering the influence of various sources and processes, such as flocculation and photodegradation, we hypothesized that these patterns may be linked to differences in SGD during flood-ebb cycles, as well as variations in total suspended matter (TSM) concentrations that affect the sorption and desorption of DBC.

Despite the significant uncertainty associated with these estimates due to the limited availability of DBC concentration data, our preliminary estimations suggest that SGD contributes approximately 12% of the riverine discharge of DBC to the JRE. This finding helps to close the mass balance between the influx and efflux of DBC in estuarine environments, underscoring the importance of SGD as a previously overlooked source.

Data Availability Statement

All the data used in this study are provided in Data set in Supporting Information S1, which include the DBC concentration, B6, B5, ΔDBC and TSM. The data set is deposited in Figshare under the license of Creative Commons Attribution 4.0 (CC BY 4.0), and can be accessed through the following link: <https://doi.org/10.6084/m9.figshare.27857970.v4> and is cited in the main text (Bao et al., 2025).

References

- Bao, H., Niggemann, J., Du, M., Zhao, W., Huang, D., Yi, Y., et al. (2023). Deciphering sources and processing of dissolved black carbon in coastal seas. *Limnology & Oceanography*, 68(11), 2562–2575. <https://doi.org/10.1002/lno.12442>
- Bao, H., Niggemann, J., Huang, D., Dittmar, T., & Kao, S. J. (2019). Different responses of dissolved black carbon and dissolved lignin to seasonal hydrological changes and an extreme rain event. *Journal of Geophysical Research: Biogeosciences*, 124(3), 479–493. <https://doi.org/10.1029/2018jg004822>
- Bao, H., Qiao, J., Zhang, R., Huang, D., Wang, B., Lin, X., & Kao, S.-J. (2022). Multiproxy probing of anthropogenic influences on the different components of dissolved organic matter in coastal rainwater. *Science of the Total Environment*, 824, 153846. <https://doi.org/10.1016/j.scitotenv.2022.153846>
- Bao, H., Zhao, W., Peng, L., Du, M., Li, K., Zhan, X., et al. (2025). Spatiotemporal variation in the dissolved black carbon concentrations in three estuaries [Dataset]. *Figshare*. <https://doi.org/10.6084/m9.figshare.27857970.v4>
- Bostick, K. W., Zimmerman, A. R., Goranov, A. I., Mitra, S., Hatcher, P. G., & Wozniak, A. S. (2021). Biolability of fresh and photodegraded pyrogenic dissolved organic matter from laboratory-prepared chars. *Journal of Geophysical Research: Biogeosciences*, 126(5). <https://doi.org/10.1029/2020jg005981>
- Cabral, A., Sugimoto, R., Taniguchi, M., Tait, D., Nakajima, T., Honda, H., & Santos, I. R. (2023). Fresh and saline submarine groundwater discharge as sources of carbon and nutrients to the Japan Sea. *Marine Chemistry*, 249, 104209. <https://doi.org/10.1016/j.marchem.2023.104209>

Acknowledgments

This work is funded by the National Key Research and Development Program of China (2024YFC2815800), National Natural Science Foundation of China (Nos: 41721005, 42076041, and 92251306), the National Science Foundation of Fujian Province (2020J05010), the Fundamental Research Funds for the Central Universities (20720200115). Bin Chen is acknowledged for his assistance in sediment sampling. Dr. Hongyan Bao acknowledges the Alexander von Humboldt Foundation for supporting her stay in Germany.

- Canuel, E. A., & Hardison, A. K. (2016). Sources, ages, and alteration of organic matter in estuaries. *Annual Review of Marine Science*, 8(1), 409–434. <https://doi.org/10.1146/annurev-marine-122414-034058>
- Cao, F., Mishra, D. R., Schalles, J. F., & Miller, W. L. (2018). Evaluating ultraviolet (UV) based photochemistry in optically complex coastal waters using the Hyperspectral Imager for the Coastal Ocean (HICO). *Estuarine, Coastal and Shelf Science*, 215, 199–206. <https://doi.org/10.1016/j.ecss.2018.10.013>
- Chen, H., Abdulla, H. A. N., Sanders, R. L., Myneni, S. C. B., Mopper, K., & Hatcher, P. G. (2014). Production of black carbon-like and aliphatic molecules from terrestrial dissolved organic matter in the presence of sunlight and iron. *Environmental Science and Technology Letters*, 1(10), 399–404. <https://doi.org/10.1021/ez5002598>
- Coppola, A. I., Druffel, E. R. M., Broek, T. A., Haghypour, N., Eglinton, T. I., McCarthy, M., & Walker, B. D. (2024). Variable aging and storage of dissolved black carbon in the ocean. *Proceedings of the National Academy of Sciences of the U S A* (Vol. 121(13), e2305030121). <https://doi.org/10.1073/pnas.2305030121>
- Coppola, A. I., Seidel, M., Ward, N. D., Viviroli, D., Nascimento, G. S., Haghypour, N., et al. (2019). Marked isotopic variability within and between the Amazon River and marine dissolved black carbon pools. *Nature Communications*, 10(1), 4018. <https://doi.org/10.1038/s41467-019-11543-9>
- Coppola, A. I., Wagner, S., Lennartz, S. T., Seidel, M., Ward, N. D., Dittmar, T., et al. (2022). The black carbon cycle and its role in the Earth system. *Nature Reviews Earth and Environment*, 3(8), 516–532. <https://doi.org/10.1038/s43017-022-00316-6>
- Coppola, A. I., Ziolkowski, L. A., Masiello, C. A., & Druffel, E. R. M. (2014). Aged black carbon in marine sediments and sinking particles. *Geophysical Research Letters*, 41(7), 2427–2433. <https://doi.org/10.1002/2013gl059068>
- Ding, Y., Cawley, K. M., da Cunha, C. N., & Jaffé, R. (2014). Environmental dynamics of dissolved black carbon in wetlands. *Biogeochemistry*, 119, 259–273. <https://doi.org/10.1007/s10533-014-9964-3>
- Dittmar, T. (2008). The molecular level determination of black carbon in marine dissolved organic matter. *Organic Geochemistry*, 39(4), 396–407. <https://doi.org/10.1016/j.orggeochem.2008.01.015>
- Dittmar, T., Koch, B., Hertkorn, N., & Kattner, G. (2008). A simple and efficient method for the solid-phase extraction of dissolved organic matter (SPE-DOM) from seawater. *Limnology and Oceanography: Methods*, 6, 230–235. <https://doi.org/10.4319/lom.2008.6.230>
- Dittmar, T., & Paeng, J. (2009). A heat-induced molecular signature in marine dissolved organic matter. *Nature Geoscience*, 2(3), 175–179. <https://doi.org/10.1038/ngeo440>
- Dittmar, T., Paeng, J., Gihring, T. M., Suryaputra, I. G. N. A., & Huettel, M. (2012). Discharge of dissolved black carbon from a fire-affected intertidal system. *Limnology & Oceanography*, 57(4), 1171–1181. <https://doi.org/10.4319/lom.2012.57.4.1171>
- Du, M., Jin, S., Wu, S., Liao, Y., & Wang, G. (2024). Hydrographic proxies for submarine groundwater discharge in the Jiulong River estuary and global perspectives. *Water Research*, 260, 121854. <https://doi.org/10.1016/j.watres.2024.121854>
- Duan, A., Zhong, Y., Xu, G., Yang, K., Tian, B., Wu, Y., et al. (2024). Quantifying the 2022 extreme drought in the Yangtze river basin using GRACE-FO. *Journal of Hydrology*, 630, 130680. <https://doi.org/10.1016/j.jhydrol.2024.130680>
- Eisma, D. (1986). Flocculation and de-flocculation of suspended matter in estuaries. *Netherlands Journal of Sea Research*, 20(2), 183–199. [https://doi.org/10.1016/0077-7579\(86\)90041-4](https://doi.org/10.1016/0077-7579(86)90041-4)
- Fang, Y., Huang, G., Chen, Y., Hu, L., Lin, J., & Lin, T. (2021). Particulate and dissolved black carbon in Bohai and Laizhou bays, China: Distributions, sources, and contrasts under two distinct fluvial hydrological regimes. *Frontiers in Earth Science*, 9, 697728. <https://doi.org/10.3389/feart.2021.697728>
- Fang, Z., Yang, W., Chen, M., & Ma, H. (2017). Source and fate of dissolved black carbon in the western south China sea during the Southwest Monsoon prevailing season. *Journal of Geophysical Research: Biogeosciences*, 122(11), 2817–2830. <https://doi.org/10.1002/2017jg004014>
- Fang, Z., Yang, W., Stubbins, A., Chen, M., Li, J., Jia, R., et al. (2021). Spatial characteristics and removal of dissolved black carbon in the western Arctic Ocean and Bering Sea. *Geochimica et Cosmochimica Acta*, 304, 178–190. <https://doi.org/10.1016/j.gca.2021.04.024>
- Fu, W., Qi, Y., Luo, C., Zhang, H., & Wang, X. (2023). Distinct radiocarbon ages reveal two black carbon pools preserved in large river estuarine sediments. *Environmental Science & Technology*, 57(15), 6216–6227. <https://doi.org/10.1021/acs.est.2c09079>
- García-Martín, E. E., Sanders, R., Evans, C. D., Kitidis, V., Lapworth, D. J., Rees, A. P., et al. (2021). Contrasting estuarine processing of dissolved organic matter derived from natural and human-impacted landscapes. *Global Biogeochemical Cycles*, 35(10). <https://doi.org/10.1029/2021gb007023>
- Goranov, A. I., Chen, H., Duan, J., Myneni, S. C. B., & Hatcher, P. G. (2024). Potentially massive and global non-pyrogenic production of condensed “black” carbon through biomass oxidation. *Environmental Science & Technology*, 58(6), 2750–2761. <https://doi.org/10.1021/acs.est.3c05448>
- Gu, H., Moore, W. S., Zhang, L., Du, J., & Zhang, J. (2012). Using radium isotopes to estimate the residence time and the contribution of Submarine Groundwater Discharge (SGD) in the Changjiang effluent plume, East China Sea. *Continental Shelf Research*, 35, 95–107. <https://doi.org/10.1016/j.csr.2012.01.002>
- Guo, X., Xu, B., Burnett, W. C., Wei, Q., Nan, H., Zhao, S., et al. (2020). Does submarine groundwater discharge contribute to summer hypoxia in the Changjiang (Yangtze) River Estuary? *Science of the Total Environment*, 719, 137450. <https://doi.org/10.1016/j.scitotenv.2020.137450>
- Hedges, J. I., Keil, R., & Benner, R. (1997). What happens to terrestrial organic matter in the ocean? *Organic Geochemistry*, 27(5–6), 195–212. [https://doi.org/10.1016/s0146-6380\(97\)00066-1](https://doi.org/10.1016/s0146-6380(97)00066-1)
- Hockaday, W. C., Grannas, A. M., Kim, S., & Hatcher, P. G. (2007). The transformation and mobility of charcoal in a fire-impacted watershed. *Geochimica et Cosmochimica Acta*, 71(14), 3432–3445. <https://doi.org/10.1016/j.gca.2007.02.023>
- Hong, Q., Cai, P., Shi, X., Li, Q., & Wang, G. (2017). Solute transport into the Jiulong River estuary via pore water exchange and submarine groundwater discharge: New insights from 224 Ra/228 Th disequilibrium. *Geochimica et Cosmochimica Acta*, 198, 338–359. <https://doi.org/10.1016/j.gca.2016.11.002>
- Huang, D., & Yu, T. (2017). Assessment of gamma radiation levels and natural radioactivity in soils along a subtropical river basin, China. *Radiochimica Acta*, 105(9), 755–762. <https://doi.org/10.1515/ract-2016-2699>
- Huovinen, P. S., Penttilä, H., & Soimasuo, M. R. (2003). Spectral attenuation of solar ultraviolet radiation in Humic lakes in Central Finland. *Chemosphere*, 51(3), 205–214. [https://doi.org/10.1016/s0045-6535\(02\)00634-3](https://doi.org/10.1016/s0045-6535(02)00634-3)
- Jaffé, R., Ding, Y., Niggemann, J., Vähätalo, A. V., Stubbins, A., Spencer, R. G. M., et al. (2013). Global charcoal mobilization from soils via dissolution and riverine transport to the oceans. *Science*, 340(6130), 345–347. <https://doi.org/10.1126/science.1231476>
- Jones, M. W., Coppola, A. I., Santin, C., Dittmar, T., Jaffe, R., Doerr, S. H., & Quine, T. A. (2020). Fires prime terrestrial organic carbon for riverine export to the global oceans. *Nature Communications*, 11(1), 2791. <https://doi.org/10.1038/s41467-020-16576-z>
- Kaiser, K., & Guggenberger, G. (2000). The role of DOM sorption to mineral surfaces in the preservation of organic matter in soils. *Organic Geochemistry*, 31(7), 711–725. [https://doi.org/10.1016/S0146-6380\(00\)00046-2](https://doi.org/10.1016/S0146-6380(00)00046-2)

- Khoo, C. L. L., Sipler, R. E., Fudge, A. R., Beheshti Foroutani, M., Boyd, S. G., & Ziegler, S. E. (2022). Salt-induced flocculation of dissolved organic matter and iron is controlled by their concentration and ratio in boreal coastal systems. *Journal of Geophysical Research: Biogeosciences*, 127(11). <https://doi.org/10.1029/2022jg006844>
- Kuzyakov, Y., Bogomolova, I., & Glaser, B. (2014). Biochar stability in soil: Decomposition during eight years and transformation as assessed by compound-specific ¹⁴C analysis. *Soil Biology and Biochemistry*, 70, 229–236. <https://doi.org/10.1016/j.soilbio.2013.12.021>
- Liu, J., Du, J., Wu, Y., & Liu, S. (2018). Nutrient input through submarine groundwater discharge in two major Chinese estuaries: The Pearl River Estuary and the Changjiang River Estuary. *Estuarine, Coastal and Shelf Science*, 203, 17–28. <https://doi.org/10.1016/j.ecss.2018.02.005>
- Manning, A. J., Langston, W. J., & Jonas, P. J. (2010). A review of sediment dynamics in the Severn estuary: Influence of flocculation. *Marine Pollution Bulletin*, 61(1–3), 37–51. <https://doi.org/10.1016/j.marpolbul.2009.12.012>
- Mannino, A., & Harvey, H. R. (2004). Black carbon in estuarine and coastal ocean dissolved organic matter. *Limnology & Oceanography*, 49(3), 735–740. <https://doi.org/10.4319/lo.2004.49.3.0735>
- Marques, J. S. J., Dittmar, T., Niggemann, J., Almeida, M. G., Gomez-Saez, G. V., & Rezende, C. E. (2017). Dissolved black carbon in the headwaters-to-ocean continuum of Paraíba Do Sul river, Brazil. *Frontiers in Earth Science*, 5. <https://doi.org/10.3389/feart.2017.00011>
- Moore, W. S. (2010). The effect of submarine groundwater discharge on the ocean. *Annual Review of Marine Science*, 2(1), 59–88. <https://doi.org/10.1146/annurev-marine-120308-081019>
- Moore, W. S., Blanton, J. O., & Joye, S. B. (2006). Estimates of flushing times, submarine groundwater discharge, and nutrient fluxes to Okeete Estuary, South Carolina. *Journal of Geophysical Research*, 111(C9). <https://doi.org/10.1029/2005jc003041>
- Moore, W. S., Sarmiento, J. L., & Key, R. M. (2008). Submarine groundwater discharge revealed by ²²⁸Ra distribution in the upper Atlantic Ocean. *Nature Geoscience*, 1(5), 309–311. <https://doi.org/10.1038/ngeo183>
- Qiao, J., Bao, H., Huang, D., Li, D.-W., Lee, T.-Y., Huang, J.-C., & Kao, S.-J. (2019). Runoff-driven export of terrigenous particulate organic matter from a small mountainous river: Sources, fluxes and comparisons among different rivers. *Biogeochemistry*, 147(1), 71–86. <https://doi.org/10.1007/s10533-019-00629-7>
- Raymond, P. A., & Bauer, J. E. (2001). DOC cycling in a temperate estuary: A mass balance approach using natural ¹⁴C and ¹³C isotopes. *Limnology & Oceanography*, 46(3), 655–667. <https://doi.org/10.4319/lo.2001.46.3.0655>
- Raymond, P. A., & Spencer, R. G. M. (2015). Riverine DOM. In *Biogeochemistry of marine dissolved organic matter* (pp. 509–533). <https://doi.org/10.1016/b978-0-12-405940-5.00011-x>
- RCoreTeam. (2022). R: A language and environment for statistical computing (version 4.1.3). In *R foundation for statistical computing*.
- Reithmaier, G. M. S., Cabral, A., Akhand, A., Bogard, M. J., Borges, A. V., Bouillon, S., et al. (2023). Carbonate chemistry and carbon sequestration driven by inorganic carbon outwelling from mangroves and saltmarshes. *Nature Communications*, 14(1), 8196. <https://doi.org/10.1038/s41467-023-44037-w>
- Roebuck, J. A., Jr., Podgorski, D. C., Wagner, S., & Jaffé, R. (2017). Photodissolution of charcoal and fire-impacted soil as a potential source of dissolved black carbon in aquatic environments. *Organic Geochemistry*, 112, 16–21. <https://doi.org/10.1016/j.orggeochem.2017.06.018>
- Schlitzer, R. (2023). Ocean data View. <https://odv.awi.de>
- Scully, M. E., & Friedrichs, C. T. (2003). The influence of asymmetries in overlying stratification on near-bed turbulence and sediment suspension in a partially mixed estuary. *Ocean Dynamics*, 53(3), 208–219. <https://doi.org/10.1007/s10236-003-0034-y>
- Seidel, M., Beck, M., Greskowiak, J., Riedel, T., Waska, H., Suryaputra, I. N. A., et al. (2015). Benthic-pelagic coupling of nutrients and dissolved organic matter composition in an intertidal sandy beach. *Marine Chemistry*, 176, 150–163. <https://doi.org/10.1016/j.marchem.2015.08.011>
- Seidel, M., Beck, M., Riedel, T., Waska, H., Suryaputra, I. G. N. A., Schnetger, B., et al. (2014). Biogeochemistry of dissolved organic matter in an anoxic intertidal creek bank. *Geochimica et Cosmochimica Acta*, 140, 418–434. <https://doi.org/10.1016/j.gca.2014.05.038>
- Stubbins, A., Niggemann, J., & Dittmar, T. (2012). Photo-lability of deep ocean dissolved black carbon. *Biogeosciences*, 9(5), 1661–1670. <https://doi.org/10.5194/bg-9-1661-2012>
- Stubbins, A., Spencer, R. G. M., Mann, P. J., Holmes, R. M., McClelland, J. W., Niggemann, J., & Dittmar, T. (2015). Utilizing colored dissolved organic matter to derive dissolved black carbon export by arctic rivers. *Frontiers in Earth Science*, 3. <https://doi.org/10.3389/feart.2015.00063>
- Turner, A., & Millward, G. E. (2002). Suspended particles: Their role in estuarine biogeochemical cycles. *Estuarine, Coastal and Shelf Science*, 55(6), 857–883. <https://doi.org/10.1006/ecss.2002.1033>
- Uher, G., Hughes, C., Henry, G., & Upstill-Goddard, R. C. (2001). Non-conservative mixing behavior of colored dissolved organic matter in a Humic-rich, turbid estuary. *Geophysical Research Letters*, 28(17), 3309–3312. <https://doi.org/10.1029/2000gl012509>
- Wagner, S., Brandes, J., Spencer, R. G. M., Ma, K., Rosengard, S. Z., Moura, J. M. S., & Stubbins, A. (2019). Isotopic composition of oceanic dissolved black carbon reveals non-riverine source. *Nature Communications*, 10(1), 5064. <https://doi.org/10.1038/s41467-019-13111-7>
- Wang, G., Wang, Z., Zhai, W., Moore, W. S., Li, Q., Yan, X., et al. (2015). Net subterranean estuarine export fluxes of dissolved inorganic C, N, P, Si, and total alkalinity into the Jiulong River estuary, China. *Geochimica et Cosmochimica Acta*, 149, 103–114. <https://doi.org/10.1016/j.gca.2014.11.001>
- Ward, N. D., Keil, R. G., Medeiros, P. M., Brito, D. C., Cunha, A. C., Dittmar, T., et al. (2013). Degradation of terrestrially derived macromolecules in the Amazon River. *Nature Geoscience*, 6(7), 530–533. <https://doi.org/10.1038/ngeo1817>
- Wu, Y., Bao, H., Yu, H., Zhang, J., & Kattner, G. (2015). Temporal variability of particulate organic carbon in the lower Changjiang (Yangtze River) in the post-Three Gorges Dam period: Links to anthropogenic and climate impacts. *Journal of Geophysical Research: Biogeosciences*, 120(11), 2194–2211. <https://doi.org/10.1002/2015jg002927>
- Yamashita, Y., Mori, Y., & Ogawa, H. (2023). Hydrothermal-derived black carbon as a source of recalcitrant dissolved organic carbon in the ocean. *Science Advances*, 9(6), eade3807. <https://doi.org/10.1126/sciadv.ade3807>
- Yamashita, Y., Nakane, M., Mori, Y., Nishioka, J., & Ogawa, H. (2022). Fate of dissolved black carbon in the deep Pacific Ocean. *Nature Communications*, 13(1), 307. <https://doi.org/10.1038/s41467-022-27954-0>
- Yang, S.-I., Ding, P.-x., & Chen, S.-I. (2001). Changes in progradation rate of the tidal flats at the mouth of the Changjiang (Yangtze) River, China. *Geomorphology*, 38(1), 167–180. [https://doi.org/10.1016/s0169-555x\(00\)00079-9](https://doi.org/10.1016/s0169-555x(00)00079-9)
- Yangtze River Water Resources Commission of the Ministry of Water Resources. (2023). *Changjiang sediment bulletin, 2022*. Changjiang Press.
- Yu, F., Zong, Y., Lloyd, J. M., Huang, G., Leng, M. J., Kendrick, C., et al. (2010). Bulk organic ^δ13C and C/N as indicators for sediment sources in the Pearl River delta and estuary, southern China. *Estuarine, Coastal and Shelf Science*, 87(4), 618–630. <https://doi.org/10.1016/j.ecss.2010.02.018>
- Zhang, Q., Zhou, J., Fang, Z., Yang, W., Chen, M., & Zheng, M. (2023). Sources and dynamics of dissolved black carbon in the Pearl River Estuary and shelf, Northern South China sea. *Journal of Oceanography*, 80(1), 71–83. <https://doi.org/10.1007/s10872-023-00708-2>

- Zhang, R., Qiao, J., Huang, D., Lin, X., Tian, L., Wang, B., et al. (2023). Seasonal variations in the sources and influential factors of aerosol dissolved black carbon at a Southeast coastal site in China. *Journal of Geophysical Research: Atmospheres*, *128*(7), e2023JD038515. <https://doi.org/10.1029/2023jd038515>
- Zhao, W., Bao, H., Huang, D., Niggemann, J., Dittmar, T., & Kao, S.-J. (2023). Evidence from molecular marker and FT-ICR-MS analyses for the source and transport of dissolved black carbon under variable water discharge of a subtropical Estuary. *Biogeochemistry*, *162*(1), 43–55. <https://doi.org/10.1007/s10533-022-00987-9>
- Ziolkowski, L. A., & Druffel, E. R. M. (2010). Aged black carbon identified in marine dissolved organic carbon. *Geophysical Research Letters*, *37*(16). <https://doi.org/10.1029/2010GL043963>